Ceramics International 47 (2021) 17276–17285

Contents lists available at ScienceDirect

Ceramics International

journal homepage: www.elsevier.com/locate/ceramint

Thickness effect on the properties of Mn-doped ZnO thin films synthesis by sol-gel and comparison to first-principles calculations

Ammar Boukhari [a,b,c], Bahri Deghfel [a,*], Abdelhafidh Mahroug [a,b], Rabie Amari [a,b], Noureddine Selmi [e], Soorathep Kheawhom [f], Ahmad Azmin Mohamad [c,d,**]

[a] Department of Physics, Faculty of Sciences, University of M'sila, Algeria
[b] Department of Mechanical Engineering, Faculty of Technology, University of M'sila, Algeria
[c] School of Materials and Mineral Resources Engineering, Universiti Sains Malaysia, 14300, Nibong, Tebal, Penang, Malaysia
[d] Ionics Materials and Devices (iMADE) Research Laboratory, Institute of Science, Universiti Teknologi MARA, 40450, Shah Alam, Malaysia
[e] Nuclear Research Center of Birine, Box 180, Ain Oussera, 17000, Algeria
[f] Department of Chemical Engineering, Faculty of Engineering, Chulalongkorn University, Bangkok, 10330, Thailand

ARTICLE INFO

Keywords:
Film thickness
Sol-gel spin coating method
Mn-doped ZnO
Structural properties
DFT+U

ABSTRACT

The current study investigates the effect of thickness on the structural, morphological, electronic, and optical properties of pure zinc oxide (ZnO) and 7% Mn-doped ZnO thin films, deposited by sol–gel spin coating method. All films exhibited a hexagonal wurtzite structure with a high preferential c-axis orientation. The surface morphology showed a good uniformity with cracks and wrinkles. The transmittance decreased with thickness. The bandgap energy was inversely varying with coating number. Photoluminescence spectra showed ultraviolet with strong and weak blue and weak green emission peaks. Density functional theory and Hubbard (DFT + U) method was then applied to study the structural, electronic, and optical properties of pure and 6.25% Mn-doped ZnO materials. A decrease in bandgap energy from pure to 6.25% Mn-doped ZnO material was shown using the DFT + U method. It also found that the Mn3d states were distributed far from Fermi level with a coexistence of both ionic and covalent nature bonds. A slight shift toward the lower energy was noticed for optical properties by Mn doping. The theoretical findings showed a similar behavior to those obtained by experiment.

1. Introduction

Zinc oxide (ZnO), a II–VI semiconductor material, has been receiving much consideration and extensively studied owing to its wide bandgap (3.37 eV) and large exciton binding energy (60 meV) [1]. Thus, its physical and chemical properties are attracting many researchers to use it in certain applications [2,3]. Different material composition, concentration, thickness, annealing temperature, and other parameters can change the structural, electronic, and optical properties of ZnO thin films, which can lead to the change in the surface morphology, particle size, orientation of crystalline structure, and concentration of defect modifications [4]. Furthermore, to improve its properties, ZnO is doped with transition metal elements such as Fe, Al, Co, and Mn [5].

ZnO doped with Mn^{+2} has a promising optical and luminescence properties such as a high optical gain (300 cm^{-1}), and very short luminescence lifetime, which are required for various optoelectronic and magneto-optical devices [6,7]. Generally, doping ZnO with Mn^{2+} keeps the wurtzite structure, which is similar in the ionic radius of Mn^{2+} (0.80 Å) and Zn^{2+} (0.74 Å) ions, facilitating the incorporation of the dopant in the host lattice [8]; however, it may cause changes in the luminescence, electronic, and optical properties of ZnO. Unlike strain and roughness, numerous studies found that the grain size, average transmittance, and bandgap values of Mn-doped ZnO thin films are less than the pure ZnO values [7,9].

The thickness effect of pure ZnO thin films was widely studied using different physical and chemical synthesis methods such as atomic layer deposition [2], pulsed laser deposition [10], filtered cathodic vacuum arc method [11], spray pyrolysis [12,13], magnetron sputtering [3,14], and sol–gel [15–19].

However, to the best of our knowledge, investigations on the thickness effect of Mn-doped ZnO thin films, which mostly used RF magnetron sputtering method for preparation, are limited [20–22]. It is worth

* Corresponding author.
** Corresponding author. School of Materials and Mineral Resources Engineering, Universiti Sains Malaysia, 14300, Nibong, Tebal, Penang, Malaysia.
E-mail addresses: bahri.deghfel@univ-msila.dz, b_deghfel@yahoo.fr (B. Deghfel), aam@usm.my (A.A. Mohamad).

https://doi.org/10.1016/j.ceramint.2021.03.039
Received 15 September 2020; Received in revised form 4 March 2021; Accepted 5 March 2021
Available online 8 March 2021

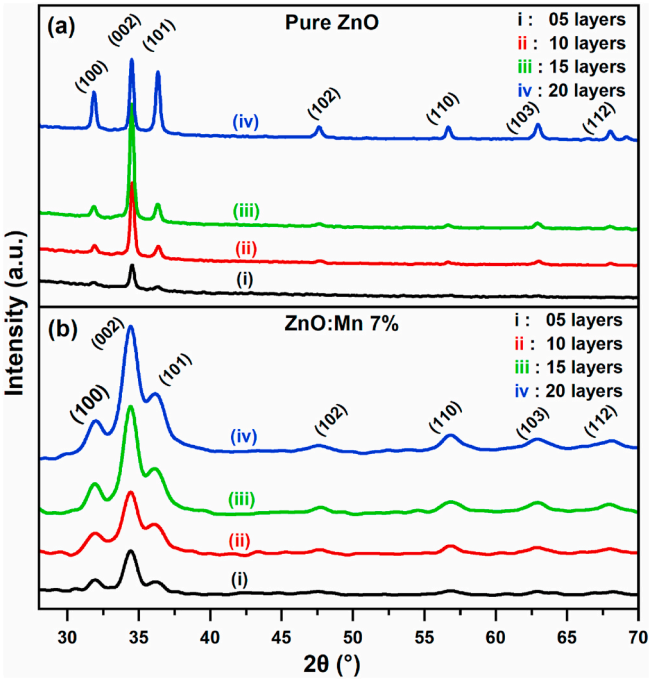

Fig. 1. XRD patterns for various deposited layers of (a) pure and (b) 7% Mn-doped ZnO thin films.

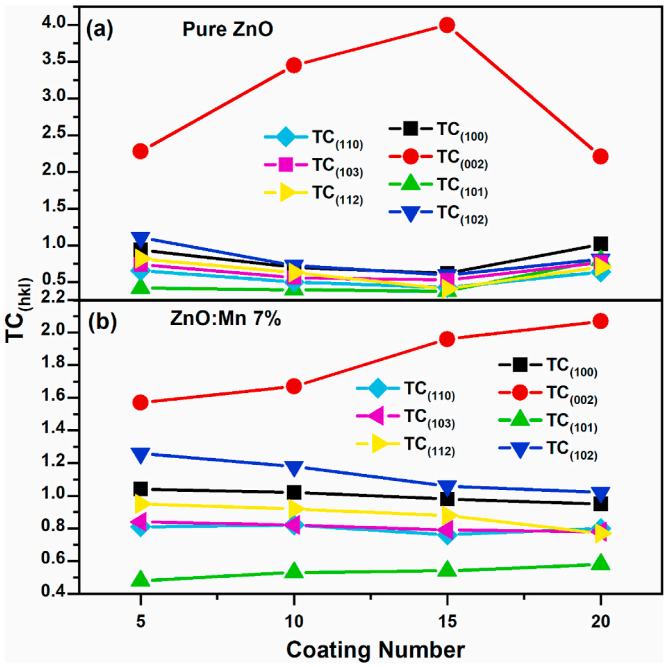

Fig. 2. Texture coefficient ($TC_{(hkl)}$) values of (a) pure and (b) 7% Mn-doped ZnO thin films for various deposited layers.

Table 1
Structural parameters of pure and 7% Mn-doped ZnO thin films for various deposited layers.

Samples	Coating number	Thickness (nm)	2θ (°)	c (Å)	FWHM (°)	Peak intensity	Crystallite size (nm)	Strain, ϵ_z (%)	Grain size from AFM (nm)
Pure ZnO	05	242	34.52	5.194	0.224	1073	37.15	−0.233	54.60
	10	609	34.54	5.192	0.218	2598	38.00	−0.284	64.86
	15	808	34.50	5.198	0.209	3870	39.63	−0.169	46.33
	20	1194	34.49	5.198	0.199	2622	41.74	−0.166	70.31
7% Mn:ZnO	05	450	34.36	5.218	0.824	614.14	10.09	0.219	46.33
	10	951	34.38	5.215	0.815	695.14	10.20	0.165	50.96
	15	1295	34.40	5.212	0.807	907.30	10.30	0.097	55.59
	20	1871	34.42	5.209	0.820	992.41	10.14	0.055	62.50

Table 2
Different structural and optical parameters of pure and Mn-doped ZnO thin films reported in the literature at different thicknesses.

Sample	Thickness	Substrate	Zn (mol/L)	Mn (%)	Method	c(Å)	CS (nm)	Strain (%)	BG (eV)	AT (%)	PO	Ref.
Pure ZnO	220	Glass	–	0	Sol–gel	–	–	0.0775	3.22	77	(101)	[51]
	227	Glass	–	0	FCVAD	5,21	22.52	−0.065	3.20	>90	(002)	[41]
	280	Glass	0.20	0	Sol–gel	–	–	–	3.245	86.9	(002)	[42]
	295	Glass	0.65	0	Sol–gel	–	19.70	−0.05	3.227	95	(002)	[38]
	500	Glass	0.30	0	Sol–gel	5,170	27.6	−0.71	3.27	80	(002)	[40]
	600	Glass	0.10	0	Sol–gel	–	–	0.47	3.272	79.21	(002)	[17]
	600	Glass	0.10	0	Spray pyrolytic	5,208	23	0.28	3.19		(101)	[12]
	910	Glass	0.10	0	Spray pyrolytic	5,203	27	0.26	3.210	60.1	(101)	[12]
	800	Glass	0.70	0	Sol–gel	5,203	31.88	0.185	3.277	85	(002)	[39]
	1300	Glass	0.016	0	Sol–gel	5,205	–	–	3.31	75	(101)	[36]
Mn-doped ZnO	398	Fused quartz	–	5	RF sputtering in nitrogen	5.210	18	0.035	3.37	57	(002)	[22]
	957	Fused quartz	–	5	gas	5.190	21	−0.303	3.34	50	(002)	[22]
	1346	Fused quartz	–	5		5.190	26	−0.246	3.31	47	(002)	[22]
	1650	Fused quartz	–	5		5.200	24	−0.218	3.03	41	(002)	[22]

Zn = Zinc concentration.
Mn = Manganese content in Zn.
C = Lattice parameter.
CS = Crystallite size.
BG = Bandgap energy.
AT = Average transmittance.
PO = Preferred orientation.

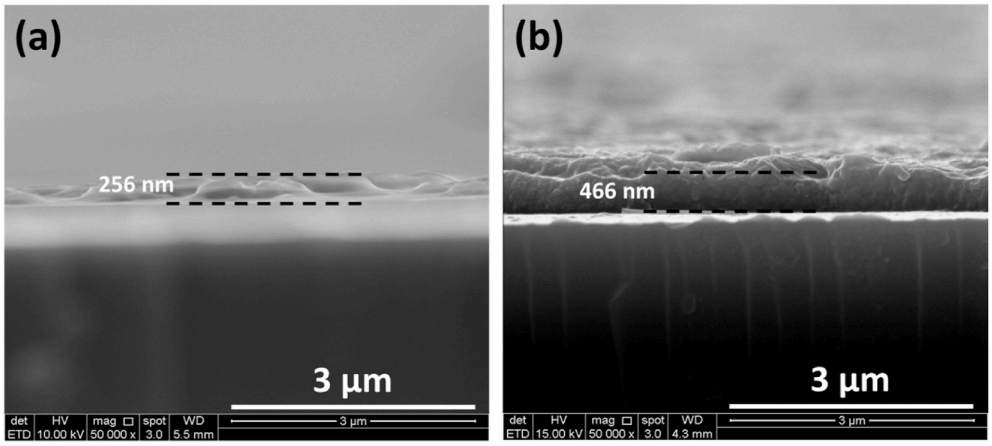

Fig. 3. FESEM cross sectional images of the samples of 5 layers; (a) pure ZnO thin films, ((b) 7% Mn-doped ZnO thin films.

noting that thickness parameter has a significant influence on the properties of pure and Mn-doped ZnO thin films. Based on the literature, for pure ZnO, studied using the sol–gel method, the films prefer the (002) c-axis orientation and crystalline wurtzite structure. By increasing the thickness (number of coats), the crystallinity improves with the increase of grain size and roughness, while the strain, average transmittance, and bandgap decreases [15,18,23]. This behavior is similar to Mn-doped ZnO prepared by RF magnetron sputtering method with thickness [20–22].

Theoretically, to predict the physical properties of pure and Mn-dope ZnO materials, few research were performed using the first-principle pseudopotential method based on density functional theory (DFT) and different forms of exchange-correlation function [24–26]. The standard DFT method failed to describe the ground-state properties of materials containing strong localized d- and f-electron metals and underestimated their fundamental bandgap and corresponding optical properties [27]. However, the DFT + U approach was then successfully applied to address this problem [28].

This study aims to investigate experimentally the influence of thickness on the structural, morphological, and optical properties of pure and 7% Mn-doped ZnO thin films. The different coating layers were deposited on glass substrates using the simple and low-cost sol–gel spin coating method. Then, the properties of pure and Mn-doped ZnO ($Zn_{1-x}Mn_xO$, x = 6.25%) were theoretically assessed using the DFT + U approach.

2. Experimental details

2.1. Preparation of the sample

The sol–gel spin coating technique was used to synthesize pure and Mn-doped ZnO thin films grown on glass substrates. Zinc acetate dehydrate [$Zn(CH_3COO)_2$–$2H_2O$] and manganese acetate tetrahydrate [$Mn(CH_3COO)_2$–$4H_2O$] were used as a precursor and source of Mn^{2+} dopant ions. For pure ZnO samples, the precursor was dissolved in isopropanol [$(CH_3)_2CHOH$]. Then, monoethanolamine [$NH_2CH_2CH_2OH$] was added to the solution as stabilizer. The molar ratio of the monoethanolamine to ion metal was fixed at 1. The solution was stirred at 65 °C for 1 h and aged at room temperature for 24 h. Then, it was deposited at a spinning rate of 2000 rpm for 30 s and then was dried. The deposition was on a glass substrate, which was cleaned in an ultrasonic bath with acetone, ethanol, and deionized water for 10 min. To evaporate the solvent and remove organic residuals, the deposited films were preheated in a furnace at 250 °C for 5 min. The process of coating and preheating was repeated to increase the film thickness. The obtained films were then annealed in air at 500 °C for 1 h. To prepare the doped films, [Mn ($CH_3COO)_2$–$4H_2O$] and [Zn ($CH_3COO)_2$–$2H_2O$] were mixed together at 7% mol concentration and were dissolved to form the solution. To deposit the Mn-doped ZnO thin films on the glass substrates, the same steps were followed as in pure ZnO.

2.2. Characterization of the samples

The film thicknesses were measured using Stylus Profilometer (model: D 500). Using an X-ray diffractometer (XRD; X'Pert PRO MPD X-ray diffractometer) with Cu-kα radiation having a wavelength of λ = 1.5406 Å, the structural properties of the films were characterized. The surface morphology of the films was observed by atomic force microscopy (AFM; model Asylum Research, MFP-3D Classic) and field emission scanning electron microscope (FESEM; Zeiss Supra 35 VP). The optical transmission spectra were measured by an ultraviolet–visible (UV–vis) spectrophotometer (UV-3101 PC-Shimadzu) in the spectral range of 350–800 nm, and the bandgap was then evaluated. Photoluminescence (PL) measurements were recorded using a spectrofluorometer (Perkin Elmer LS 50B) with the excitation wavelength of 325 nm.

3. Computational details

The 2 × 2 × 4 ZnO supercell containing 64 atoms is constructed from the optimized bulk wurtzite ZnO unit cell. Then, two Mn atoms substitutionally replaced two nearest Zn sites to achieve the concentration x = 6.25%, and antiferromagnetic phase was considered. For the practical, x = 6.25% of Mn concentration was used as it is the nearest value to 7% (concentration of Mn in the experimental part), which offers a less time-consuming DFT calculation. This was confirmed in the previous works for x = 12.5% [29,30], where Mn atoms form cluster around the O atom. The obtained supercells of pure and Mn-doped ZnO materials ($Zn_{1-x}Mn_xO$; x = 6.25%) are optimized using DFT as implemented in CASTEP code [31]. The generalized gradient approximation (GGA) in the scheme of Perdew–Burke–Ernzerhof (PBE) was used to treat the exchange-correlation function [32].

Valence electron configurations for constructing pseudopotential were as follows: O: $2s^2$ $2p^4$, Zn: $3d^{10}$ $4s^2$, and Mn: $3d^5$ $4s^2$. The plane-wave ultrasoft pseudopotential method was used to reduce the cut-off kinetic energy [33], which was fixed at 400 eV. The 3 × 3 × 1 k-point grid was employed for the Brillouin-zone integration. Geometric optimization was performed using the convergence thresholds of 5 × 10^{-6} eV/atom for total energy, 0.05 eV/Å for maximum force, 0.05 GPa for pressure, and 1.0 × 10^{-3} Å for maximum displacement. The total tolerance of self-consistent calculations was 5 × 10^{-6} eV/atom. Based on the semi-empirical GGA + U approach to improve the bandgap energy [34], the following effective Hubbard U values were used: 5.5 eV for *Zn 3d* states, 10 eV for *Mn 3d* states, and 8 eV for *O 2p* states.

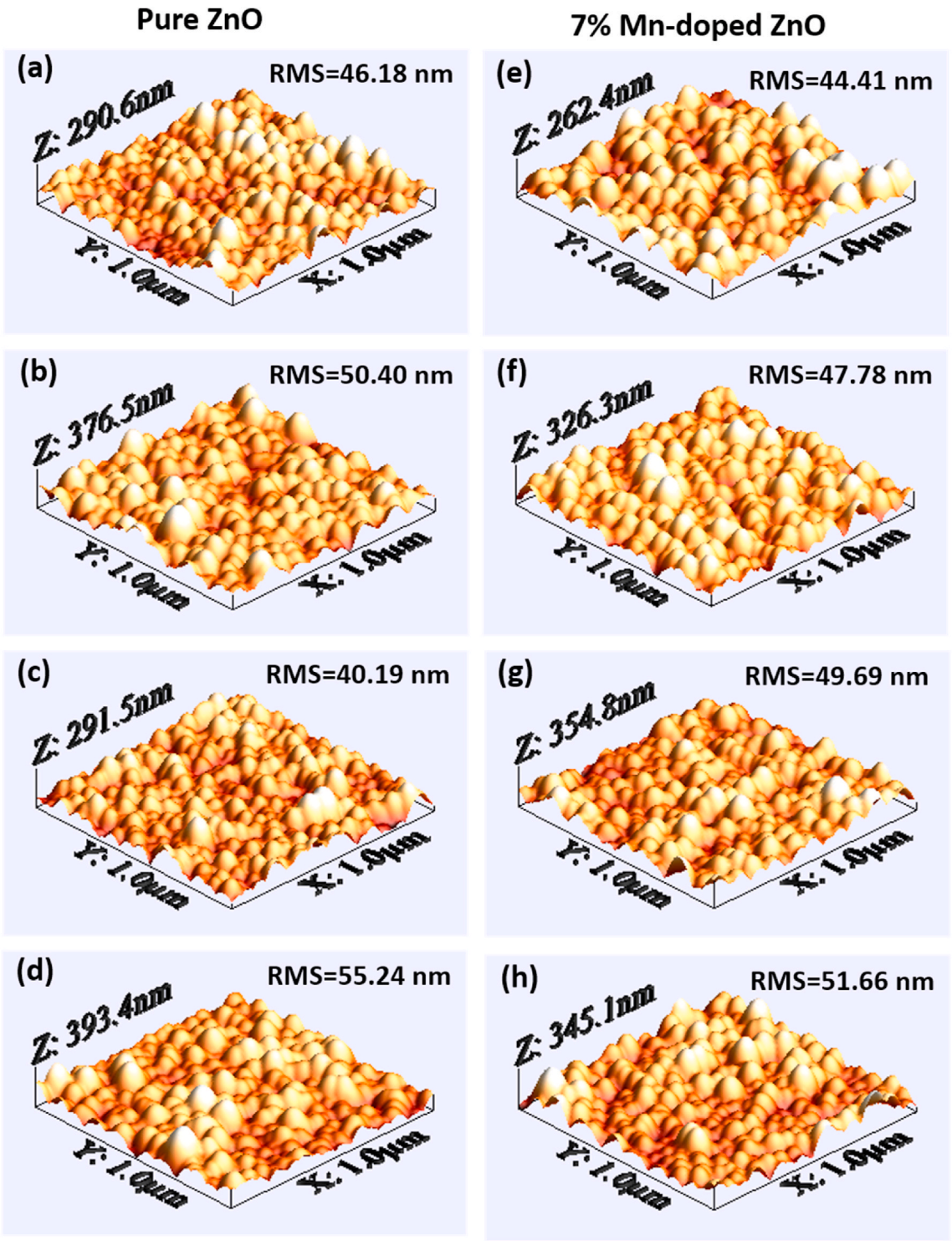

Fig. 4. 3D AFM images of pure ZnO thin films: (a) 5, (b) 10, (c) 15, and (d) 20 layers. 3D AFM images of 7% Mn-doped ZnO thin films: (e) 5, (f) 10, (g) 15, and (h) 20 layers.

4. Results and discussion

4.1. Structural properties

The structural properties of pure (Fig. 1a) and Mn-doped ZnO (Fig. 1b) were studied by XRD, and three main peaks were observed: (100), (002), and (101). These peaks indicate that the pure and Mn-doped ZnO thin films are polycrystalline with a preferential orientation along the c-axis. No secondary phase (impurity) was formed in the doped films, such as $ZnMnO_3$ [20]. It was also shown that Mn^{+2} substituted for Zn^{2+} of ZnO host does not change the wurtzite structure [6].

However, it is observed that the (002) diffraction peak is stronger than the other peaks, indicating that the common direction along the c-axis is the preferential growth direction. Another factor is that the surface free energy of (002) planes is the most stable compared to others [35]. The diffraction peaks become broader for Mn-doped ZnO thin films because of the increase of strain due to Mn^{+2} incorporation in the Zn

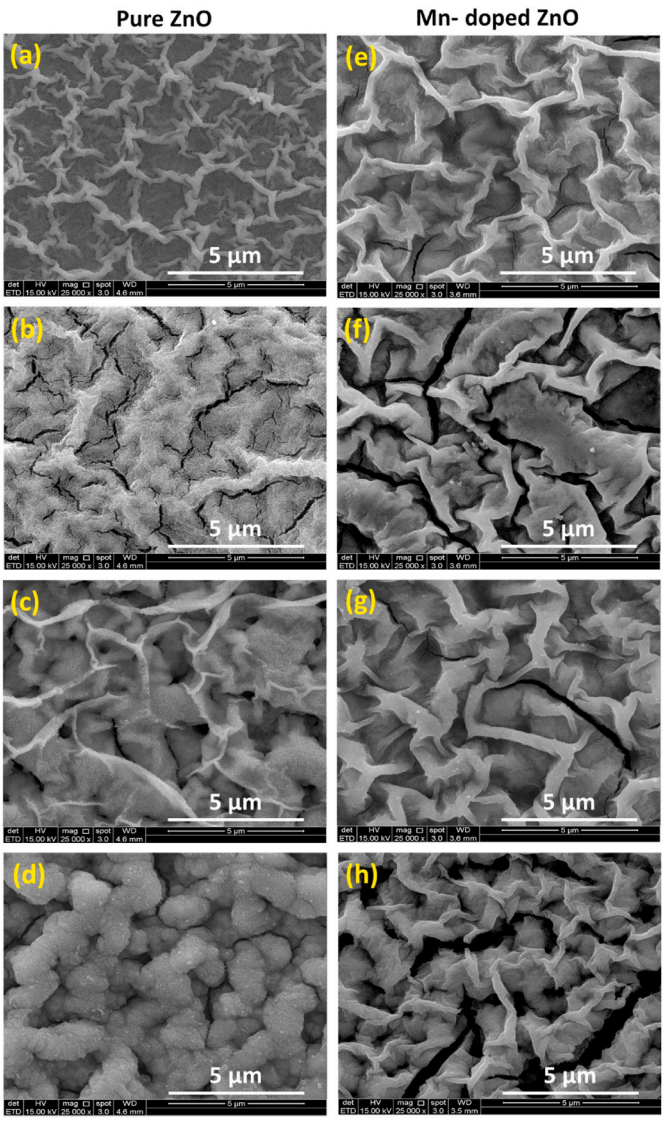

Fig. 5. FESEM images of pure ZnO thin films: (a) 5, (b) 10, (c) 15, and (d) 20 layers. FESEM images of 7% Mn-doped ZnO thin films: (e) 5, (f) 10, (g) 15, and (h) 20 layers.

lattice site [6,36]. The obtained results are confirmed by the large values of the strain of Mn-doped ZnO thin films compared to those of the undoped ones for all deposited layers.

The lattice constants $a = b$ and c of the thin films with different deposited layers are calculated using the structure factor for wurtzite structure [37]. The c-axis constant shifts toward higher values when going from the pure ZnO thin films to the doped ones (Table 1). This can be attributed to the fact that the ionic radius of Mn^{2+} (0.80 Å) is larger than that of Zn^{2+} (0.74 Å). The c-axis constant of Mn-doped ZnO thin films slightly decreases with the increase in coating number and approaches the bulk value 5.207 Å (JCPDS 36–1451) [7]; however, it insignificantly increases with thickness for pure ZnO thin films. This evolution is inversely proportional to the slight shift toward the lower angles of the (002) peak 2θ position with the increase of the coating number caused by relaxation of the residual strain [21]. The c-axis values at maximum relative deviation up to 0.42% (pure ZnO) and 0.52% (Mn-doped ZnO) agree well with those reported in the literature [12,22,38–41].

The average crystallite size was calculated using the full-width-at-half-maximum (FWHM) of the most intense peak (002) by Scherrer's formula for pure and Mn-doped ZnO films with various thicknesses (Table 1). It can be seen that the values of crystallite size of pure ZnO films are higher than those of Mn-doped films for all deposited layers. This may be due to the strain induced in the doped ZnO caused by the replacement of the host (Zn^{2+}) by the dopant (Mn^{2+}) cations that prevents the grain growth [6,9].

Furthermore, for pure ZnO thin films, the calculated values of the crystallite sizes strongly depend on the number of the deposited layers and increase when the number of the deposited layers increases; however, for Mn-doped ZnO thin films, these values slightly vary and generally tend to increase as the number of deposited layers increases. It is worth noting that a similar behavior of the crystallite sizes was observed by others for pure ZnO thin films synthesized by sol–gel [16,42] and for 5% Mn-doped ZnO films synthesized by RF sputtering in nitrogen gas [22].

The strain (ε_{ZZ}) values are calculated using the following equation [40]:

$$\varepsilon_{ZZ} = [(c - c_0) / c_0].100\% \quad (1)$$

where c is the lattice parameter of the strained films estimated from the X-ray diffraction data and c_0 is the unstrained lattice parameter of bulk ZnO (Table 1). The compressive strain decreases with the increase of the film thickness for pure thin films, where the film is relaxed and becomes thicker. However, Mn-doped thin films present a decreasing tensile strain.

Most of the results reported in literature (Table 2), generally present a similar behavior by increasing the thickness compared to those found in the present study (Table 1). The values are not close to our results due to deposition method, Mn concentration, or thickness differences. The most effective peaks on XRD were further analyzed by texture coefficient $TC_{(hkl)}$ estimated using the following relation [38]:

$$TC_{(hkl)} = \frac{I_{(hkl)}}{I_{0(hkl)}} \Big/ \frac{1}{N}\sum_{1}^{N}\left(\frac{I_{(hkl)}}{I_{0(hkl)}}\right) \quad (2)$$

where $I_0(hkl)$ is the intensity of the standard powder diffraction peak, N is the number of diffraction peaks, and $I(hkl)$ is the measured relative intensity of a diffraction peak.

The texture coefficient $TC_{(hkl)}$ for all peaks observed in XRD patterns of pure (Fig. 2a) and Mn-doped ZnO (Fig. 2b) thin films were calculated for various thicknesses. The highest $TC_{(hkl)}$ value was in the (002) plane for both pure and Mn-doped ZnO thin films, indicating that all films present a preferred growth orientation along c-axis, i.e., (002) plane, whatever the number of the deposited layers is. The degree of c-axis orientation depends on the number of the deposited layers where the higher value of texture coefficient reveals a better crystallinity of thin film. It can be seen that the intensity of (002) diffraction peak is increased as the film is grown up to 15 layers for both pure and Mn-doped ZnO thin films. Above 15 layers, unlike the pure ZnO thin films, where the (002) peak was decreased, the (002) intensity peak continued to increase for Mn-doped ZnO thin films. The intensity of (100) and (101) peaks were found to be increased with coating numbers for both pure and doped ZnO films. However, the $TC_{(hkl)}$ values for the main peak (002) of the Mn-doped ZnO thin films slightly vary in the range of 1.57–2.07 with the number of deposited layers.

4.2. Morphological properties

It is observed that the film thickness was increased with coating number, especially for Mn-doped thin films (Table 1). The average thickness of each layer was found to be 50 nm for pure ZnO and 90 nm for Mn-doped ZnO (Fig. 3). To investigate the morphological properties of pure and Mn-doped ZnO thin films with various thicknesses, AFM (Fig. 4) and FESEM analyses (Fig. 5) were used. The 3D AFM images were scanned over an area of 1.0 × 1.0 µm^2. The grain size and surface roughness of samples were extracted from the AFM images (Table 1)

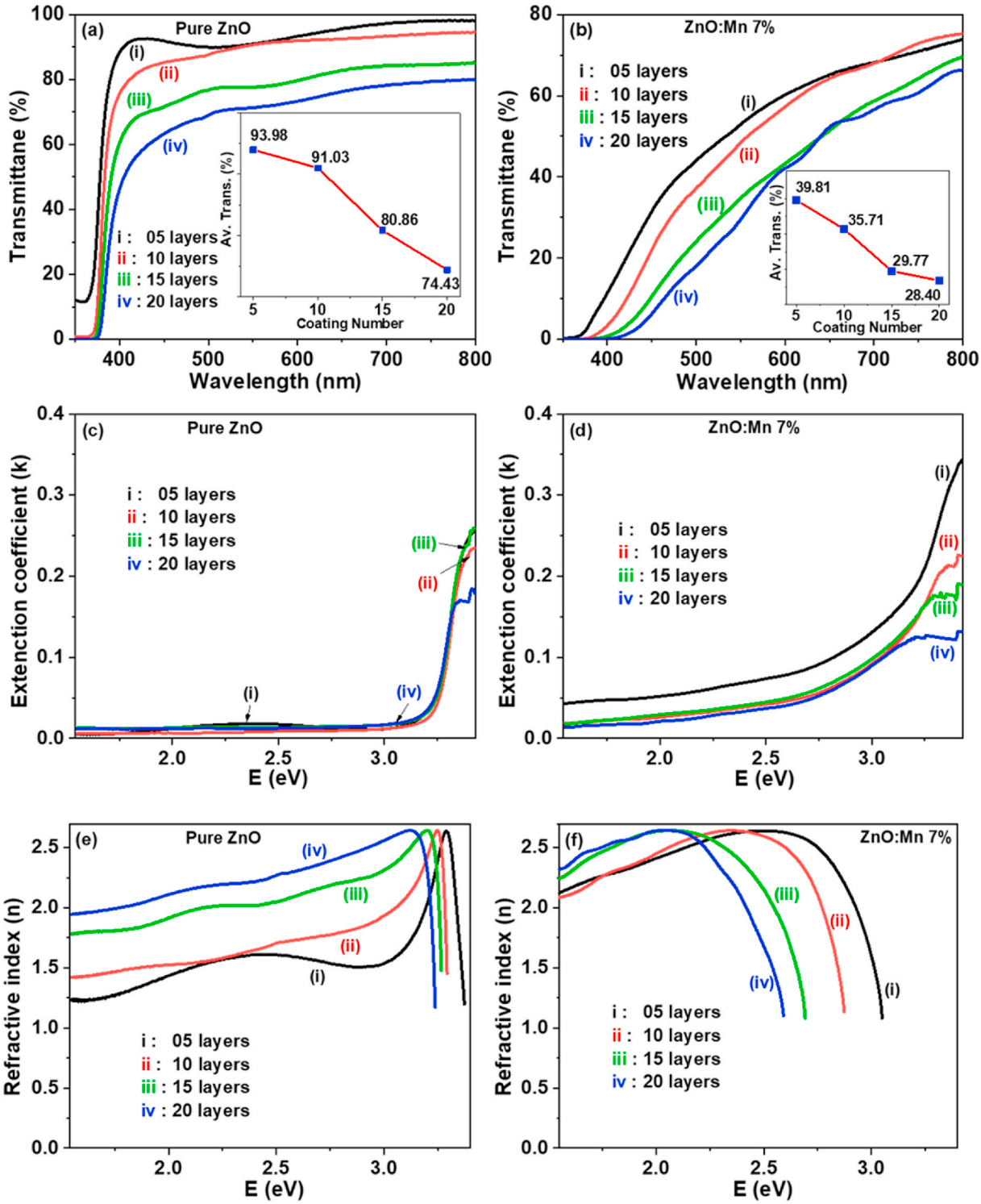

Fig. 6. Transmittance spectra (a, b), extinction coefficient (c, d) and refractive index (e, f) of pure and 7% Mn-doped ZnO thin films for various deposited layers. Inset in (a) and (b) shows average transmittance (Av. Trans.).

using WsXM software [43]. The samples present a uniform growth, the grains are round shape in plane for all samples, and their size generally increases by increasing the coating number for both doped and pure ZnO thin films. This means that the grain growth is mainly vertical and then tends to become lateral by increasing the film thickness, which agrees with our XRD analysis. The ZnO thin films involve columnar grains that grow along the (002) direction perpendicular to the substrate surface. The surface roughness of the films was found to be increased with thickness.

A wrinkled microstructure was observed in the FESEM images of pure and Mn-doped ZnO thin films, which is distributed homogenously over the whole film surface. As the thickness increased, the width, length, and height of wrinkles were increased. Also, cracks appeared from the samples of 10 layers for both pure (Fig. 5b) and Mn-doped ZnO (Fig. 5f), whereas the samples of 5 layers are without cracks. The width of cracks increased with increasing thickness. Similar surface shape was

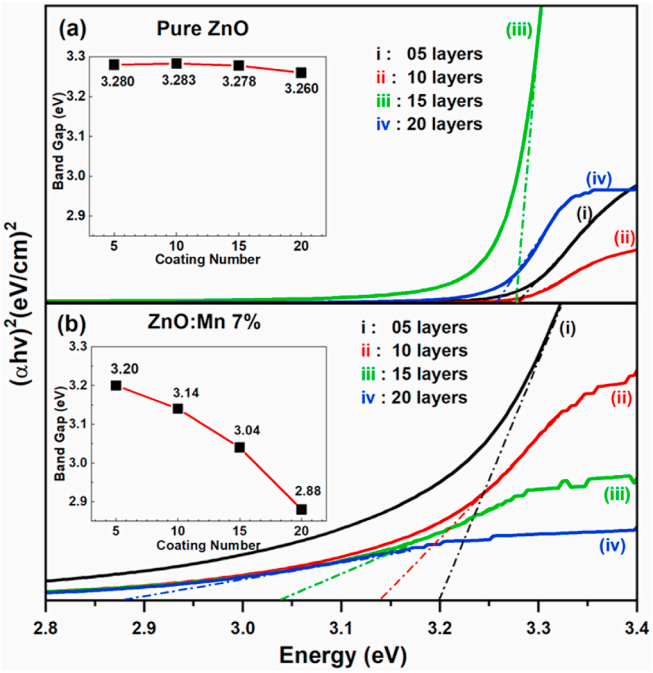

Fig. 7. $(\alpha h\nu)^2$ versus photon energy $h\nu$ of (a) pure and (b) 7% Mn-doped ZnO thin films for various deposited layers. Bandgap variation was also shown in the inset.

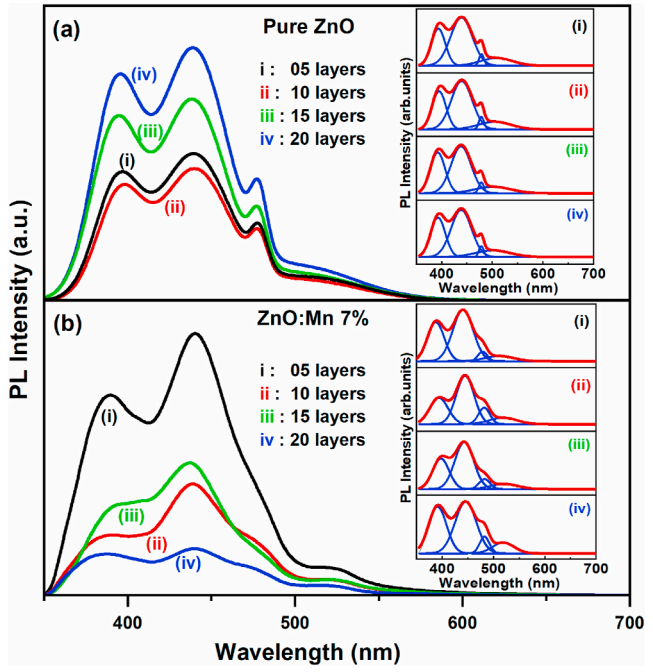

Fig. 8. PL spectra of (a) pure and (b) 7% Mn-doped ZnO thin films for various deposited layers. Multi-peak Gaussian fits were also shown in the inset.

observed for pure ZnO [44,45], and Ni-doped ZnO [46].

4.3. Optical properties

To investigate the effect of film thickness on the optical properties of pure (Fig. 6a) and Mn-doped (Fig. 6b) ZnO thin films, UV–vis spectra were measured in the wavelength range of 350–800 nm at room temperature. In the visible region, the transmittance generally decreases with the increase of coating number for both pure and Mn-doped ZnO thin films.

The average transmittance values of the pure ZnO thin films (inset of Fig. 6a) are higher than those of Mn-doped ZnO ones (inset of Fig. 6b) at the same coating number, indicating a good visible transparency for pure ZnO thin films. This may be due to the increase in optical scattering caused by the decrease of grain size for Mn-doped thin films [2]. It is well known that the film becomes thicker as the coating number increases, which may affect the scattering of light and then decreases the transmittance for pure ZnO thin films [15,16,42].

However, a sharp (pure ZnO films) and blunt (Mn-doped ZnO films) absorption edge was observed. By increasing the thickness, a red shift of the absorption edge was observed for both pure and Mn-doped thin films. For the pure ZnO films, the slight shift toward the large wavelengths could be attributed to the decrease of the carrier concentration ascribed to the increase in the grain size and the enhancement of the crystalline quality [19]. This result shows that the bandgap slightly decreases from 3.28 to 3.26 eV as the film thickness increases.

Optical constants such as refractive index (n) and extinction coefficient (k) can be determined from the transmittance data by using the following equations [47–49]:

$$A = \log(1/T) \tag{3}$$

$$R = 1 - A - T \tag{4}$$

$$\alpha = 2.303\ \ A/t \tag{5}$$

$$k = \alpha\lambda/4\pi \tag{6}$$

$$n = (1+R)\Big/(1-R) + \sqrt{4R/(1-R)^2 - k^2} \tag{7}$$

where T is the transmittance, R is the reflectance, A is the absorbance, t is the film thickness, α is the absorption coefficient and λ is the wavelength. The variation of k and n is presented for pure (Fig. 6c and e) and Mn-doped (Fig. 6d and f) ZnO thin films. For all the films, the refractive index varies sharply near the optical edge and tends to be constant for the medium and low energy in the visible region. By increasing the coating number (thickness), the refractive index increases and shifts to lower values of energy with an appreciable amount for Mn-doped ZnO thin films than for pure ZnO thin films. The decrease in crystallite size of Mn-doped ZnO thin films compared to the pure ones (Table 1) causes an increase in film density and then an increase in refractive index [49]. Also, the optical absorption edges for the extinction coefficient are clearly seen and predict a noticeable variation of band gap with coating number for Mn-doped ZnO than pure ZnO. These findings exhibit a similar behavior to those calculated by other researchers for pure ZnO [41,47,48,50] and sometimes they are in agreement with them despite the different elaboration method and the film thickness [49].

The absorption coefficient, previously calculated, was then used to evaluate the bandgap (E_g) by utilizing the Tauc's equation [39]. The $(\alpha h\nu)^2$ vs. photon energy $h\nu$ for both pure (Fig. 7a) and Mn-doped (Fig. 7b) ZnO thin films were plotted for various deposited layers. The bandgap values for the pure ZnO thin films (inset of Fig. 7a) are higher than those of the Mn-doped ZnO (inset of Fig. 7b). This may be attributed to the shrinking of the bandgap caused by the merging of an impurity band near the conduction band caused by the exchange interaction between localized states of the transition metal ions and s-p states of the host band [6,36]. For pure ZnO thin films, the bandgap slightly decreases from 3.28 to 3.26 eV when the coating number is increased from 5 to 20. There was a slight deviation (up to 2.07%) in the energy bandgap from our results compared with those reported in previous works (Table 2).

However, the bandgap decreases with appreciable variation from 3.20 to 2.88 eV for Mn-doped thin films. The observed deviation, which

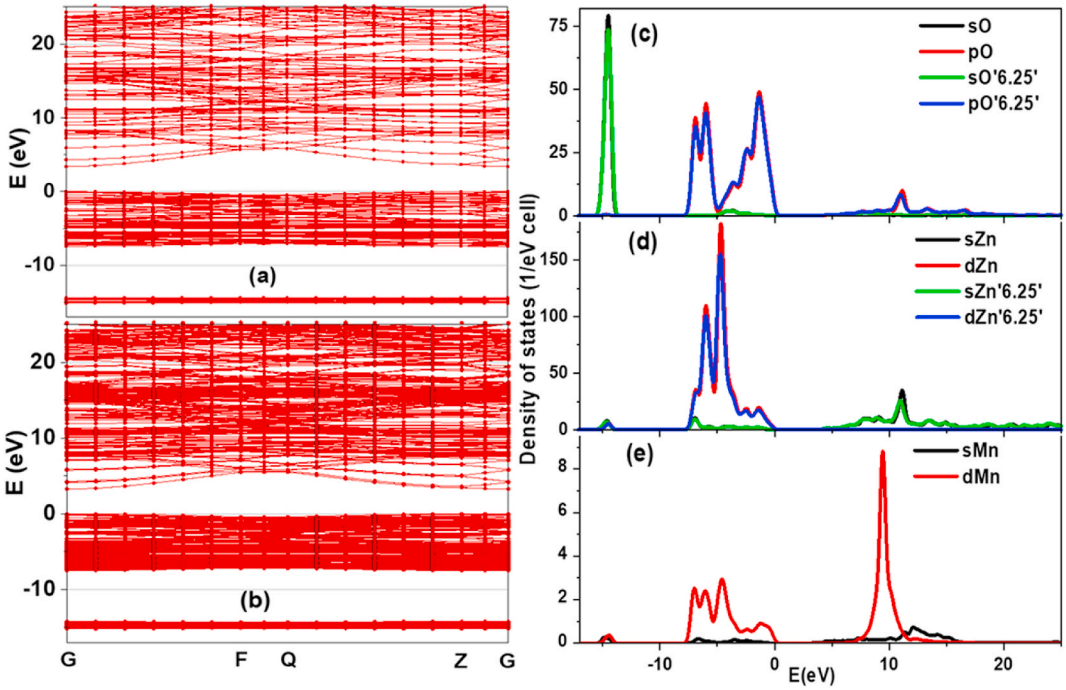

Fig. 9. Band structure of pure (a) and Mn-doped (b) ZnO structures and partial density of States (PDOS); (c) O 2s, O2p, (d) Zn 4s, Zn 3d, (e) Mn 4s and Mn 3d states.

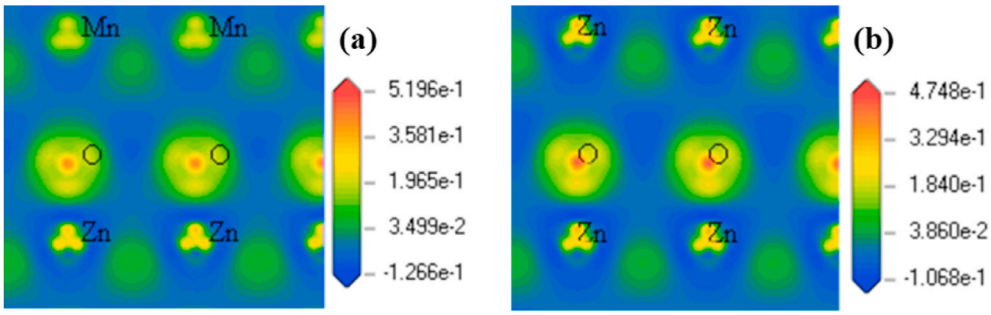

Fig. 10. Distribution (010) surface of charge density difference for (a) pure and (b) Mn-doped ZnO.

is somewhat higher (up to 8.88%), is attributed to the fact that the bandgap values are taken from 5% Mn-doped ZnO concentration [22]. The bandgap variation for both pure and Mn-doped ZnO might be due to the change in the strain along the c-axis [22,42].

The effect of the coating number on the PL properties of pure (Fig. 8a) and Mn-doped (Fig. 8b) ZnO thin films were investigated. The obtained experimental data of PL spectra were fitted by multi-peak Gaussian shape (insets of Fig. 8). In the pure and doped thin film spectra, two major peaks were shown: the near-band-edge emission centered at 387 nm, which is due to free exciton emission [39], and broad blue emission centered at 439 nm. A second blue emission at around 475 nm can be seen for both pure and Mn-doped ZnO thin films, but it becomes more pronounced for pure ZnO thin films and vanishes progressively for Mn-doped ZnO thin films with thickness. This indicates that the oxygen vacancy concentration is decreased for Mn-doped ZnO thin films with thickness, which may be due to the formation of multi-layer Mn segregation in ZnO grain boundary [52]. The samples also show a weak green emission with a peak centered at 525 nm.

However, the origin of these emissions has not been decisively understood where many researchers suggested various origins for the same peak in the visible emission region [53–55]. The broad and strong blue emission at around 439 nm could be originated from transition from interstitial Zn_i to the valence band; the second blue emission may be attributed to the electron transition from the oxygen vacancy level to the valence band; and the green emission, as quoted by some researchers, may be due to the transition from conduction band to the O_{Zn} level [53, 56].

As the film thickness increases, the intensity of the visible emission increases for pure ZnO thin films, which is affected by the appreciable change in the grain size and defect concentration of the pure ZnO [6,16]. Unlike pure ZnO, the intensities of the visible emission of the doped thin films inversely vary as the coating number increases.

4.4. First-principle calculation

The optimized lattice constants of pure (a = b = 3.236 Å and c = 5.202 Å) and Mn-doped (a = b = 3.255 Å and c = 5.238 Å) ZnO structures are slightly increased with Mn concentration, which are comparable with our experimental results. To analyze the electronic properties, the energy band structures (Fig. 9a and b) and partial density of O2s, O2p, Zn 4s, Zn 3d, Mn 4s and Mn 3d states, PDOS, (Fig. 9c, d and e), are shown for pure and Mn-doped ZnO structures. It is observed that both structures are direct band gap at G point; Eg = 3.381 eV for ZnO and Eg = 3.246 eV for Mn-doped ZnO. However, the incorporation of the semi-empirical GGA + U approach with appropriate effective Hubbard U values improves significantly the theoretical direct bandgap values

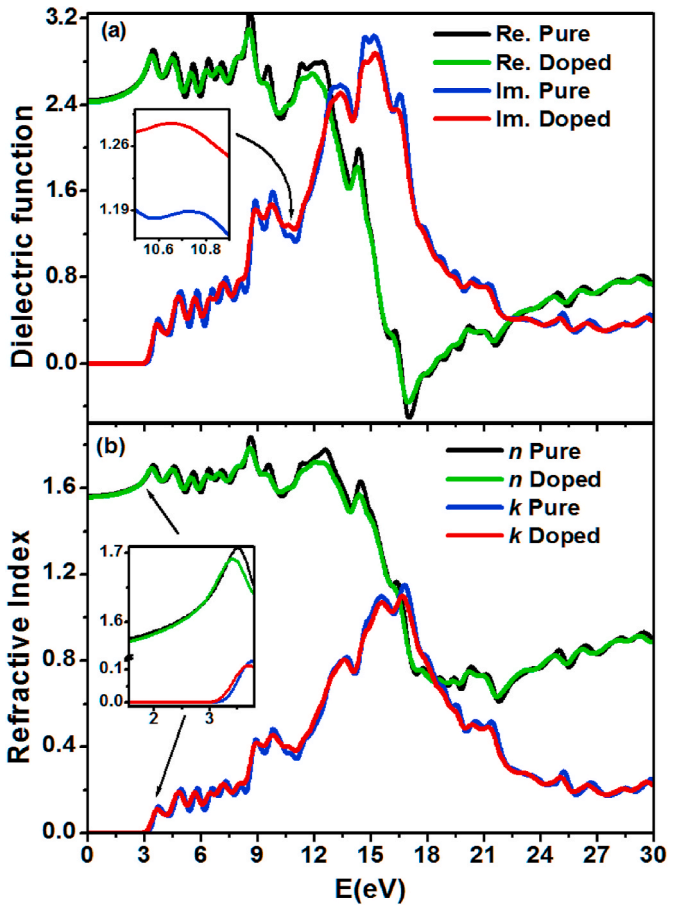

Fig. 11. Complex dielectric function (a) and refractive index, *n*, and extinction coefficient, *k*, (b) for pure ZnO and Mn-doped ZnO structures. Inset in (a) shows dielectric function within the energy range 10.5–10.9 eV. Inset in (b) shows *n* and *k* within the visible range of photon energy.

compared to our values obtained without taking into account the Hubbard correction (Eg = 0.742 eV for ZnO and Eg = 0.003 eV for Mn-doped ZnO) and to other previous results [30,57].

By incorporating Mn atoms, the conduction band, which mainly originates from Zn *4s* with some mixture of Mn *3d*, O *2p* states, and a little Mn *4s* effect, was shrunk and shifts downward to Fermi level, which slightly decreases the bandgap (Fig. 9c, d and e). On the other hand, the top of valence band appears to be relatively flat within a region of 7.5 eV and is mainly from mixture of O *2p* and Zn *3d* states with a little contribution from Mn *3d* states. These latter states seem to be distributed far from Fermi level.

The average Mulliken charges are found to be as follows: for pure ZnO, Zn: 0.950e, and O: −0.950e, and for Mn-doped ZnO, Zn: 0.955e, Mn: 0.960e, and O: −0.954e. Then, the effective valence of Zn is 1.050 for pure ZnO and that of Zn is 1.045 and Mn is 1.040 for Mn-doped ZnO. This indicates the coexistence of both ionic and covalent bonding either for pure or Mn-doped ZnO structures.

The distribution (010) surfaces of charge density difference were studied for pure (Fig. 9a) and Mn-doped (Fig. 10b) ZnO. Yellow regions show charge loss (depletion), red regions represent charge accumulation, and blue color indicates a region with minimal difference. This is consistent with the results obtained for the atomic population; the more the atom has effective valence, the more it attracts electrons.

The frequency-dependent dielectric function is the main parameter to deduce the optical properties of materials [58,59]. Both pure and Mn-doped ZnO present similar behavior in the complex dielectric function presentation (Fig. 11a). The peak intensities of pure material are all slightly higher than those of Mn-doped material because of the replacement of Zn atoms by Mn ones. There is an exception within a narrow energy range (10.5–10.9 eV), where a peak is appeared at around 10.7 eV (insets of Fig. 11a). This peak may be mainly derived from the transition between the O *2p* and Mn *3d* orbitals. The shrinking of bandgap energy for doped material causes a slight shift of dielectric function toward the lower energy of incident photon.

The calculated refractive index and extinction coefficient are also shown (Fig. 11b) for pure and Mn-doped ZnO structures. The extinction coefficient presents a sharp increase near the optical edge with slight shift to lower energy for Mn-doped ZnO structure (Inset in Fig. 11b). The refractive index tends to be constant for lower photon energy in the visible region (around 1.56 for pure and 1.55 for Mn-doped ZnO structure). Both refractive index and extinction coefficient exhibit a similar behavior to those deduced from experiment in this work within the considered energy range of the incident photon (1.55–3.5 eV).

5. Conclusions

"The thickness effects of pure and 7% Mn-doped ZnO thin films on glass substrates, obtained by sol-gel spin coating method, were characterized and calculated by GGA + U. All films present a polycrystalline hexagonal wurtzite structure with a preferential orientation along the (002) axis. A uniform growth and round shape in plane of grains are observed, and their grain size slightly increases by increasing the thickness. A wrinkled microstructure is homogeneously distributed in pure and Mn-doped ZnO thin films, whose roughness is found to be increased with thickness. The transmittance and bandgap were found to be decreased for both pure and doped ZnO films with thickness, where the bandgap slightly decreases for the pure ZnO films. The high PL properties are remarked at low thickness for Mn-doped ZnO films and at high thickness for pure ZnO films. The GGA + U approach improves the theoretical direct bandgap values. The covalency of bonds is slightly influenced from pure to Mn-doped ZnO structure, and both ionic and covalent bonding are coexisted. Combination of experimental and theoretical from this work will shed light on designing Mn-doped ZnO thin films for optical, sensors and solar cell applications".

Declaration of competing interest

The authors declare that they have no known competing financial interests or personal relationships that could have appeared to influence the work reported in this paper.

Acknowledgment

The authors would like to thank the Malaysian Ministry of Higher Education and appreciate the financial support provided by the Fundamental Research Grant Scheme (FRGS/1/2020/TK0/USM/02/4) (203.PBAHAN.6071467). B. Deghfel and A. Boukhari would like to thank the Algerian Ministry of Higher Education and Scientific Research for financial support under the Exceptional National Program (ENP).

References

[1] M. Soylu, M. Coskun, Controlling the properties of ZnO thin films by varying precursor concentration, J. Alloys Compd. 741 (2018) 957–968.
[2] D. Pal, J. Singhal, A. Mathur, A. Singh, S. Dutta, S. Zollner, S. Chattopadhyay, Effect of substrates and thickness on optical properties in atomic layer deposition grown ZnO thin films, Appl. Surf. Sci. 421 (2017) 341–348.
[3] A. Namoune, T. Touam, A. Chelouche, Thickness, annealing and substrate effects on structural, morphological, optical and waveguiding properties of RF sputtered ZnO thin films, J. Mater. Sci. Mater. Electron. 28 (2017) 12207–12219.
[4] A. Mahroug, R. Amari, A. Boukhari, B. Deghfel, L. Guerbous, N. Selmi, Synthesis, structural, morphological, electronic, optical and luminescence properties of pure and manganese-doped zinc oxide nanostructured thin films: effect of doping, J. Nanoelectron. Optoelectron. 13 (2018) 732–742.
[5] B. Ghanbari Shohany, A. Khorsand Zak, Doped ZnO nanostructures with selected elements - structural, morphology and optical properties: a review, Ceram. Int. 46 (2020) 5507–5520.

[6] S. Yang, Y. Zhang, Structural, optical and magnetic properties of Mn-doped ZnO thin films prepared by sol–gel method, J. Magn. Magn Mater. 334 (2013) 52–58.
[7] X. Li, X. Zhu, K. Jin, D. yang, Study on structural and optical properties of Mn-doped ZnO thin films by sol-gel method, Opt. Mater. 100 (2020) 109657.
[8] S. Aksoy, Y. Caglar, Synthesis of Mn doped ZnO nanopowders by MW-HTS and its structural, morphological and optical characteristics, J. Alloys Compd. 781 (2019) 929–935.
[9] M. Shatnawi, A.M. Alsmadi, I. Bsoul, B. Salameh, M. Mathai, G. Alnawashi, G. M. Alzoubi, F. Al-Dweri, M.S. Bawa'aneh, Influence of Mn doping on the magnetic and optical properties of ZnO nanocrystalline particles, Results Phys. 6 (2016) 1064–1071.
[10] V. Kumar, S.K. Singh, H. Sharma, S. Kumar, M.K. Banerjee, A. Vij, Investigation of structural and optical properties of ZnO thin films of different thickness grown by pulsed laser deposition method, Phys. B Condens. Matter 552 (2019) 221–226.
[11] L. Miao, S. Tanemura, M. Tanemura, S.P. Lau, B.K. Tay, Thickness-dependent optical properties of ZnO thin films, J. Mater. Sci. Mater. Electron. 18 (2007) S343–S346.
[12] T. Prasada Rao, M.C. Santhoshkumar, Effect of thickness on structural, optical and electrical properties of nanostructured ZnO thin films by spray pyrolysis, Appl. Surf. Sci. 255 (2009) 4579–4584.
[13] A. Mortezaali, O. Taheri, Z.S. Hosseini, Thickness effect of nanostructured ZnO thin films prepared by spray method on structural, morphological and optical properties, Microelectron. Eng. 151 (2016) 19–23.
[14] K. Kandpal, J. Singh, N. Gupta, C. Shekhar, Effect of thickness on the properties of ZnO thin films prepared by reactive RF sputtering, J. Mater. Sci. Mater. Electron. 29 (2018) 14501–14507.
[15] N. Kakati, S.H. Jee, S.H. Kim, J.Y. Oh, Y.S. Yoon, Thickness dependency of sol-gel derived ZnO thin films on gas sensing behaviors, Thin Solid Films 519 (2010) 494–498.
[16] L. Xu, X. Li, Y. Chen, F. Xu, Structural and optical properties of ZnO thin films prepared by sol–gel method with different thickness, Appl. Surf. Sci. 257 (2011) 4031–4037.
[17] S. Mridha, D. Basak, Effect of thickness on the structural, electrical and optical properties of ZnO films, Mater. Res. Bull. 42 (2007) 875–882.
[18] L. Cui, G.-G. Wang, H.-Y. Zhang, R. Sun, X.-P. Kuang, J.-C. Han, Effect of film thickness and annealing temperature on the structural and optical properties of ZnO thin films deposited on sapphire (0001) substrates by sol–gel, Ceram. Int. 39 (2013) 3261–3268.
[19] M. Bouderbala, S. Hamzaoui, B. Amrani, A.H. Reshak, M. Adnane, T. Sahraoui, M. Zerdali, Thickness dependence of structural, electrical and optical behaviour of undoped ZnO thin films, Phys. B Condens. Matter 403 (2008) 3326–3330.
[20] Z.N. Kayani, F. Nazir, S. Riaz, S. Naseem, Structural, optical and magnetic properties of manganese zinc oxide thin films prepared by sol–gel dip coating method, Superlattice. Microst. 82 (2015) 472–482.
[21] R. Rajalakshmi, S. Angappane, Effect of thickness on the structural and optical properties of sputtered ZnO and ZnO:Mn thin films, J. Alloys Compd. 615 (2014) 355–362.
[22] M. Venkaiah, R. Singh, Effect of thickness on structural, optical and mechanical properties of Mn doped ZnO nanocrystalline thin films RF sputtered in nitrogen gas environment, Superlattice. Microst. 72 (2014) 164–171.
[23] M.F. Malek, M.H. Mamat, T. Soga, S.A. Rahman, S. Abu Bakar, A.S. Ismail, R. Mohamed, S.A.H. Alrokayan, H.A. Khan, M.R. Mahmood, Thickness-controlled synthesis of vertically aligned c-axis oriented ZnO nanorod arrays: effect of growth time via novel dual sonication sol–gel process, Jpn. J. Appl. Phys. 55 (2015), 01AE15.
[24] M.V. Gallegos, C.R. Luna, M.A. Peluso, L.C. Damonte, J.E. Sambeth, P.V. Jasen, Effect of Mn in ZnO using DFT calculations: magnetic and electronic changes, J. Alloys Compd. 795 (2019) 254–260.
[25] M.F. Kasim, A.K.A.b. Darman, M.K. Yaakob, N. Badar, N. Kamarulzaman, Experimental and first-principles DFT studies on the band gap behaviours of microsized and nanosized Zn(1−x)MnxO materials, Phys. Chem. Chem. Phys. 21 (2019) 19126–19146.
[26] L. Wu, T. Hou, Y. Wang, Y. Zhao, Z. Guo, Y. Li, S.-T. Lee, First-principles study of doping effect on the phase transition of zinc oxide with transition metal doped, J. Alloys Compd. 541 (2012) 250–255.
[27] V.I. Anisimov, J. Zaanen, O.K. Andersen, Band theory and Mott insulators: Hubbard U instead of Stoner I, Phys. Rev. B 44 (1991) 943.
[28] M. Yaakob, N. Hussin, M. Taib, T. Kudin, O. Hassan, A. Ali, M. Yahya, First principles LDA+ U calculations for ZnO materials, Integrated Ferroelectrics Int. J. 155 (2014) 15–22.
[29] Z. Long, L. Peng-Fei, Y. Zhong-Yuan, M. Shi-Jia, D. Lu, L. Jian-Tao, The electronic and magnetic properties of (Mn, C)-codoped ZnO diluted magnetic semiconductor, Chin. Phys. B 21 (2012), 097103.
[30] R. Amari, B. Deghfel, A. Mahroug, A.A. Mohamad, A. Boukhari, N. Selmi, Effects of Mn doping on the structural, morphological, electronic and optical properties of ZnO thin films by sol-gel spin coating method: an experimental and DFT+U study, Phys. B Condens. Matter 577 (2020) 411766.
[31] S.J. Clark, M.D. Segall, C.J. Pickard, P.J. Hasnip, M.I. Probert, K. Refson, M. C. Payne, First principles methods using CASTEP, Z. für Kristallogr. - Cryst. Mater. 220 (2005) 567–570.
[32] J.P. Perdew, K. Burke, M. Ernzerhof, Generalized gradient approximation made simple, Phys. Rev. Lett. 77 (1996) 3865–3868.
[33] D. Vanderbilt, Soft self-consistent pseudopotentials in a generalized eigenvalue formalism, Phys. Rev. B 41 (1990) 7892–7895.
[34] K. Harun, N.A. Salleh, B. Deghfel, M.K. Yaakob, A.A. Mohamad, DFT + U calculations for electronic, structural, and optical properties of ZnO wurtzite structure: a review, Results Phys. 16 (2020) 102829.
[35] M. Xin, L.Z. Hu, D.-P. Liu, N.-S. Yu, Effect of Mn doping on the optical, structural and photoluminescence properties of nanostructured ZnO thin film synthesized by sol–gel technique, Superlattice. Microst. 74 (2014) 234–241.
[36] U.N. Maiti, P.K. Ghosh, S. Nandy, K.K. Chattopadhyay, Effect of Mn doping on the optical and structural properties of ZnO nano/micro-fibrous thin film synthesized by sol–gel technique, Phys. B Condens. Matter 387 (2007) 103–108.
[37] A. Mahroug, S. Boudjadar, S. Hamrit, L. Guerbous, Structural, morphological and optical properties of undoped and Co-doped ZnO thin films prepared by sol–gel process, J. Mater. Sci. Mater. Electron. 25 (2014) 4967–4974.
[38] M. Saleem, L. Fang, H. Ruan, F. Wu, Q. Huang, C. Xu, C. Kong, Effect of zinc acetate concentration on the structural and optical properties of ZnO thin films deposited by Sol-Gel method, Int. J. Phys. Sci. 7 (2012) 2971–2979.
[39] R. Amari, A. Mahroug, A. Boukhari, B. Deghfel, N. Selmi, Structural, optical and luminescence properties of ZnO thin films prepared by sol-gel spin-coating method: effect of precursor concentration, Chin. Phys. Lett. 35 (2018), 016801.
[40] D. Raoufi, T. Raoufi, The effect of heat treatment on the physical properties of sol–gel derived ZnO thin films, Appl. Surf. Sci. 255 (2009) 5812–5817.
[41] E.Ş. Tüzemen, S. Eker, H. Kavak, R. Esen, Dependence of film thickness on the structural and optical properties of ZnO thin films, Appl. Surf. Sci. 255 (2009) 6195–6200.
[42] V. Kumar, N. Singh, R. Mehra, A. Kapoor, L. Purohit, H. Swart, Role of film thickness on the properties of ZnO thin films grown by sol-gel method, Thin Solid Films 539 (2013) 161–165.
[43] I. Horcas, R. Fernández, J. Gomez-Rodriguez, J. Colchero, J. Gómez-Herrero, A. Baro, WSXM: a software for scanning probe microscopy and a tool for nanotechnology, Rev. Sci. Instrum. 78 (2007), 013705.
[44] N. Kaneva, A. Bojinova, K. Papazova, D. Dimitrov, I. Svinyarov, M. Bogdanov, Effect of thickness on the photocatalytic properties of ZnO thin films, Bulg. Chem. Commun. 47 (2015) 395–401.
[45] C.-Y. Tsay, K.-S. Fan, S.-H. Chen, C.-H. Tsai, Preparation and characterization of ZnO transparent semiconductor thin films by sol–gel method, J. Alloys Compd. 495 (2010) 126–130.
[46] N. Kaneva, C. Dushkin, Preparation of nanocrystalline thin films of ZnO by sol-gel dip coating, Bulg. Chem. Commun. 43 (2011) 259–263.
[47] S. Sharma, C. Periasamy, P. Chakrabarti, Thickness dependent study of RF sputtered ZnO thin films for optoelectronic device applications, Electron. Mater. Lett. 11 (2015) 1093–1101.
[48] M. Mazhdi, J. Saydi, M. Karimi, J. Seidi, F. Mazhdi, A study on optical, photoluminescence and thermoluminescence properties of ZnO and Mn doped-ZnO nanocrystalline particles, Optik 124 (2013) 4128–4133.
[49] Y. Caglar, Sol–gel derived nanostructure undoped and cobalt doped ZnO: structural, optical and electrical studies, J. Alloys Compd. 560 (2013) 181–188.
[50] T.P. Rao, M.S. Kumar, S.A. Angayarkanni, M. Ashok, Effect of stress on optical band gap of ZnO thin films with substrate temperature by spray pyrolysis, J. Alloys Compd. 485 (2009) 413–417.
[51] R. Gayen, K. Sarkar, S. Hussain, R. Bhar, A. Pal, ZnO films prepared by modified sol-gel technique, Indian J. Pure Appl. Phys. 49 (2011) 470–477.
[52] B. Straumal, S. Protasova, A. Mazilkin, A. Myatiev, P. Straumal, G. Schütz, E. Goering, B. Baretzky, Ferromagnetic properties of the Mn-doped nanograined ZnO films, J. Appl. Phys. 108 (2010), 073923.
[53] L. Xu, G. Zheng, J. Miao, F. Xian, Dependence of structural and optical properties of sol–gel derived ZnO thin films on sol concentration, Appl. Surf. Sci. 258 (2012) 7760–7765.
[54] M. Baneto, A. Enesca, Y. Lare, K. Jondo, K. Napo, A. Duta, Effect of precursor concentration on structural, morphological and opto-electric properties of ZnO thin films prepared by spray pyrolysis, Ceram. Int. 40 (2014) 8397–8404.
[55] R. Karmakar, S.K. Neogi, A. Banerjee, S. Bandyopadhyay, Structural; morphological; optical and magnetic properties of Mn doped ferromagnetic ZnO thin film, Appl. Surf. Sci. 263 (2012) 671–677.
[56] Y.-J. Choi, H.-H. Park, A simple approach to the fabrication of fluorine-doped zinc oxide thin films by atomic layer deposition at low temperatures and an investigation into the growth mode, J. Mater. Chem. C 2 (2014) 98–108.
[57] Z.-W. Jin, Y.-Z. Yoo, T. Sekiguchi, T. Chikyow, H. Ofuchi, H. Fujioka, M. Oshima, H. Koinuma, Blue and ultraviolet cathodoluminescence from Mn-doped epitaxial ZnO thin films, Appl. Phys. Lett. 83 (2003) 39–41.
[58] Q.-J. Liu, Z.-T. Liu, J.-C. Chen, L.-P. Feng, H. Tian, First-principles study of structural, mechanical, electronic and optical properties of 3R- and 2H-CuGaO2, Phys. B Condens. Matter 406 (2011) 3377–3382.
[59] K. Harun, N. Mansor, M.K. Yaakob, M.F.M. Taib, Z.A. Ahmad, A.A. Mohamad, On the verification of sol–gel-derived ZnO nanoparticle properties using first-principles calculation, J. Sol. Gel Sci. Technol. 80 (2016) 56–67.